
FEW-SHOT SEMANTIC SEGMENTATION VIA MASK AGGREGATION

Wei Ao

School of Remote Sensing and
Information Engineering, Wuhan
University, Wuhan, 430079, China
wei_ao@whu.edu.cn

Shunyi Zheng*

School of Remote Sensing and
Information Engineering, Wuhan
University, Wuhan, 430079, China
syzheng@whu.edu.cn

Yan Meng

School of Computer Science,
Wuhan University, Wuhan
430072, China
mengyan@whu.edu.cn

ABSTRACT

Few-shot semantic segmentation aims to recognize novel classes with only very few labelled data. This challenging task requires mining of the relevant relationships between the query image and the support images. Previous works have typically regarded it as a pixel-wise classification problem. Therefore, various models have been designed to explore the correlation of pixels between the query image and the support images. However, they focus only on pixel-wise correspondence and ignore the overall correlation of objects. In this paper, we introduce a mask-based classification method for addressing this problem. The mask aggregation network (MANet), which is a simple mask classification model, is proposed to simultaneously generate a fixed number of masks and their probabilities of being targets. Then, the final segmentation result is obtained by aggregating all the masks according to their locations. Experiments on both the PASCAL-5ⁱ and COCO-20ⁱ datasets show that our method performs comparably to the state-of-the-art pixel-based methods. This competitive performance demonstrates the potential of mask classification as an alternative baseline method in few-shot semantic segmentation. Our source code will be made available at <https://github.com/TinyAway/MANet>.

Keywords Few-shot segmentation · Mask classification · Semantic segmentation

1 Introduction

Semantic segmentation, which aims to generate dense image predictions by assigning a precise category to each pixel of the processed image, is a fundamental problem in computer vision. In recent years, great breakthroughs have been made due to the rapid development of deep convolutional neural networks (DCNNs) [Lecun and Bottou, 1998]. Through end-to-end supervised training, deep learning models can quickly acquire the ability to recognize various kinds of objects. Although methods that are based on DCNNs [Long et al., 2015, Ronneberger et al., 2015, Badrinarayanan et al., 2017, Zhao et al., 2017, Fu et al., 2019] can obtain good results, they often rely on a large number of annotated images. The performance of the model will deteriorate when there are not adequate training samples.

To address this problem, Shaban et al. [2017] first established a benchmark for few-shot segmentation (FSS). In contrast to regular semantic segmentation methods, which can only segment categories that are included in the training set, FSS methods aim to recognize unseen categories with very few annotated data. The general strategy for tackling the FSS task is to utilize meta-learning. The training data are divided into many episodes, each of which includes one query image and one or a few corresponding annotated support images. Through learning from these episodes, the model can find clues that are related to the query image from the support images and, thus, segment novel classes. Therefore, the key challenge of the FSS task is to exploit information from support images. Recent studies [Zhang et al., 2019, Wang et al., 2019, Tian et al., 2020, Yang et al., 2020a, Liu et al., 2020a] have generally utilized a two-branch architecture (see Fig. 1) to process both the support images and the query image. The support branch aims to learn prototypes from image-label pairs using masked global average pooling (GAP) Zhou et al. [2016], while the query branch is responsible for segmenting the query images by densely comparing the query features and the prototypes. In this way, the recognition ability of the model is no longer limited to the categories that appear in the training set.

*corresponding author

Although established methods can achieve good results in FSS, they are all pixel-based, which is not in line with the way human beings perceive objects because humans are better at recognizing whole objects than parts of objects. Therefore, to address this issue, we attempt to explore the association of whole objects between the query image and the support images. Inspired by mask classification methods [He et al., 2017, Hariharan et al., 2014, Kirillov et al., 2019, Cheng et al., 2021], we enable the model to automatically generate a set of masks of all the objects in the query image. Then, the problem of FSS can be transformed into determining whether the masks correspond to the foreground or background.

In this paper, a mask aggregation network (MANet), which is a simple but effective model, is proposed for tackling the challenges of FSS via mask classification. Similar to the previous FSS methods, we also adopt a two-branch structure, which includes a mask branch and a category branch (see Fig. 1). The mask branch aims to generate a set of binary masks by decoding the query features, while the category branch calculates the probability that each mask is the target by comparing the query features and the support prototypes. All the masks will be aggregated according to their locations to produce the final segmentation result. Finally, to enable the two branches to achieve their goals, a grid loss is designed to guide the model to produce correct masks. Comprehensive experiments on the PASCAL-5ⁱ and COCO-20ⁱ datasets are conducted to evaluate the performance of our method. In summary, the main contributions of this paper are threefold:

- Based on the perception of whole objects, we develop a novel two-branch model that can solve the problem of FSS by aggregating local mask information. To the best of our knowledge, we are the first to use mask classification for FSS.
- By leveraging an elaborate grid loss, our model converges well during training and can more accurately extract the masks and the corresponding categories of objects.
- The proposed method achieves competitive results on the PASCAL-5ⁱ dataset (mIoU: 61.2% for 1-shot and 64.5% for 5-shot segmentation) and COCO-20ⁱ dataset (mIoU: 36.4% for 1-shot and 44.2% for 5-shot segmentation), which provides compelling evidence that mask classification is an effective method for FSS.

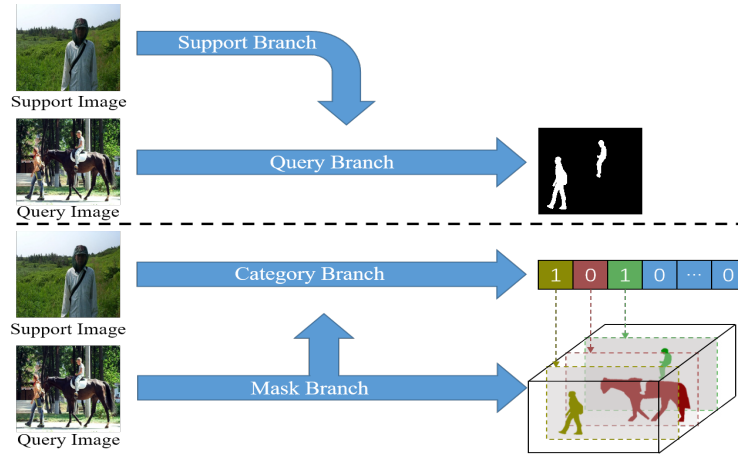


Figure 1: Comparison between the pixel-based few-shot segmentation framework (top) and our proposed mask-based method (bottom). Typical FSS methods focus on classifying all the pixels of the query image through the relevance to the support images. Our method attempts to generate a set of masks and assign them exact categories simultaneously.

2 Related work

2.1 Semantic segmentation

Semantic segmentation requires dense prediction of pixels, which is a widely studied problem in the field of computer vision. Mainstream segmentation methods [Ronneberger et al., 2015, Badrinarayanan et al., 2017, Chen et al., 2018, Noh et al., 2015] typically employ an encoder-decoder structure to realize end-to-end training. The encoder extracts high-dimensional semantic features at low resolution along the convolutional pathways, while the decoder gradually recovers the resolution of the feature maps and obtains a segmentation mask through upsampling blocks. Based on this structure, variants have been proposed for obtaining more accurate results. In U-Net [Ronneberger et al., 2015], skip

connections are added between the encoder and the decoder to decrease the loss of scale information in the encoding process. DeepLab V3+ [Chen et al., 2018] uses several convolution kernels with different scales to accurately capture the spatial information of high-level semantic feature maps. DANet [Fu et al., 2019] leverages two different attention modules to learn the spatial and channel interdependencies of features. Although these methods have been shown to be effective, they can achieve good results only if many labelled samples are available for training. Moreover, a dramatic decrease in accuracy occurs when they are used to segment unseen classes.

2.2 Few-shot segmentation

The objective of few-shot segmentation is to obtain helpful information from few labelled data for segmenting query images that contain novel classes. Recent works often formulate FSS from the perspective of metric learning. PL [Dong and Xing, 2018] produces a prototype for each class via GAP. The segmentation result is obtained by comparing the support prototypes and the query features. In PANet [Wang et al., 2019], it is assumed that a good FSS model should be able to not only segment the query image through a prototype of the support image but also correctly segment the support image by calculating a prototype of the query image. Therefore, it uses a prototype alignment strategy to fully exploit the support knowledge. CANet [Zhang et al., 2019] uses the convolution operation instead of cosine similarity to adaptively obtain the correlation between the query features and the support features. PFENet [Tian et al., 2020] considers that high-level layers of the encoder can provide rich semantic information. It leverages an extra prior map that is generated from high-level semantic information to further guide the subsequent segmentation steps. The methods that are discussed above are all pixel-based, which obtain segmentation results by comparing the features of the pixels in the query image and the features of the target pixels in the support image. However, they are unstable and easily make mistakes when the query image and the support image differ substantially.

2.3 Mask classification

Mask classification is usually used in instance segmentation tasks. To segment all the individual objects, a DCNN is usually employed to automatically generate a set of masks, which are much more numerous than the objects. Mask R-CNN [He et al., 2017] utilizes a region proposal network (RPN) to generate bounding boxes and then extracts foreground areas from them using an FCN. SOLO [Wang et al., 2020a] divides the image into regions, each of which generates a binary mask for the object in it. DETR [Carion et al., 2020] further adopts a small fixed number of learnable positional embeddings to transform an image sequence into a mask sequence. However, the accuracies of these methods are limited due to their dependence on object bounding boxes. Recently, MaskFormer [Cheng et al., 2021] was proposed, which attempts to represent all the pixels of a category as a mask; this enables mask classification to be used in semantic segmentation. Following this strategy, our model automatically generates masks of all the objects and then divides each mask into foreground or background by making dense comparisons on the query features and the support prototypes.

3 Problem setting

The objective of few-shot segmentation is to train a model that can segment unseen classes with only one or a few annotated data. Suppose that the model is trained on a dataset D_{train} with class set C_{train} ; the goal is to evaluate the model on another dataset D_{test} with class set C_{test} , where $C_{train} \cap C_{test} = \emptyset$. In contrast to the common training mode of semantic segmentation, which directly inputs the training samples into the model, in our method, both the training set and the testing set are divided into many episodes. Each episode consists of a query set $Q = (I^q, M^q)$ and a support set $S = (I_i^s, M_i^s)_{i=1}^K$, where I^* and M^* are the image and its corresponding mask, respectively, and K denotes the number of support images. During training, the model iteratively and randomly samples episodes from D_{train} to learn a mapping from the support set S and query image I^q to the query mask M^q . Then, the trained model is evaluated on the testing set in the same way.

4 Our method

In this section, we introduce the architecture of the proposed method and its loss function. Fig. 2 illustrates the structure of our proposed MANet. We adopt an encoder-decoder architecture, as is used in most FSS methods. A well-trained encoder (ResNet [He et al., 2016] pre-trained on ImageNet [Krizhevsky et al., 2012]) is used to extract high-dimensional features of the query and support images, and then a decoder is leveraged to predict the final mask by computing the correlation between the query features and the support features. However, in contrast to other FSS methods, as discussed above, we employ a mask classification method to obtain the final prediction. Herein, inspired by YOLO [Redmon et al., 2016], each query image is divided into an $S \times S$ grid. If the centre of an object falls within a grid cell, then this

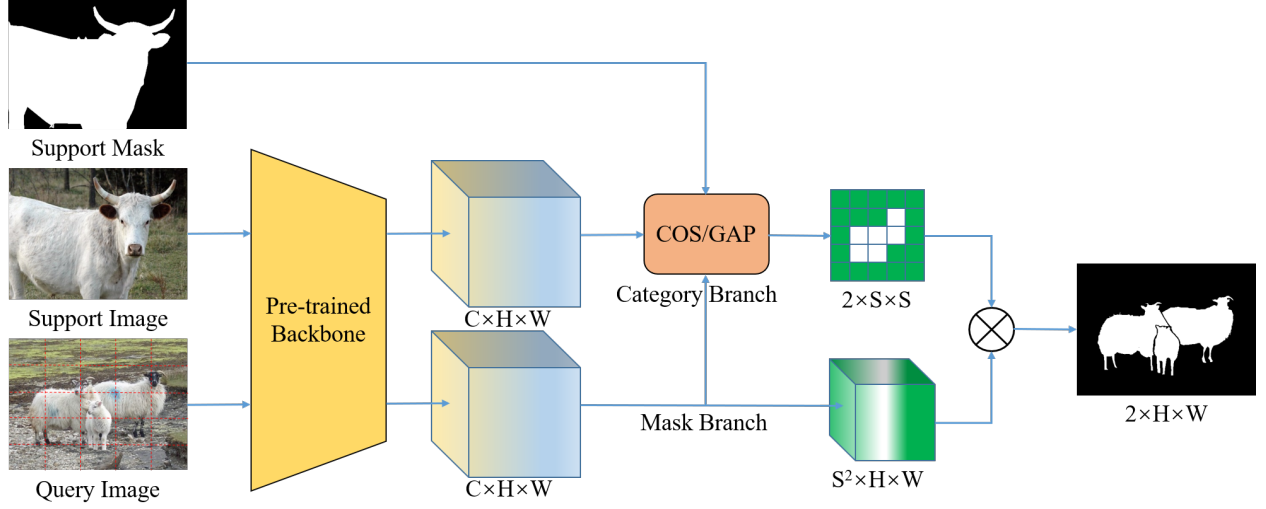


Figure 2: Overview of the proposed MANet. The query image is divided into an $S \times S$ grid. The query image and the support image are first input into a pre-trained backbone network to obtain the query features and the support features, respectively. The cosine similarity of high-level features is calculated to obtain correlation maps, and masked GAP is employed on middle-level features to generate prototypes. Then, the model is divided into two branches. The category branch aims to predict the category of the objects in each grid cell. The mask branch generates a total of S^2 masks for all the grid cells. Finally, the segmentation result is produced by matrix multiplication of the categories and the masks.

grid cell is responsible for extracting the mask and the category of this object. We introduce a two-branch structure for implementing both tasks, which includes a category branch and a mask branch. The purpose of the category branch is to determine whether the object in each grid cell corresponds to the foreground or background, and the mask branch is used to obtain a binary mask of the object in each grid cell. Finally, all the masks are aggregated according to their location information via simple matrix multiplication. Moreover, a grid loss is designed to enable the two branches to perform their respective functions. Our model is presented in detail in the following.

4.1 Category branch

The category branch is used to obtain the categories to which the objects in each grid cell belong. This branch has three inputs: query feature maps, an expanded prototype and a correlation map. The query feature maps are the middle-level semantic features that are extracted from the query image by the encoder. The dimension of each feature map is compressed to 256 via a 1×1 convolution operation. The prototype is obtained by using masked GAP for middle-level support features. Then, it is expanded to the same size as the query feature maps. The correlation map is similar to the prior mask that is used in PFENet [Tian et al., 2020]. First, the cosine similarity C_Q is calculated between high-level query features $x_q \in x_Q$ and support features $x_s \in x_S$ as

$$\cos(x_q, x_s) = \frac{x_q^T x_s}{\|x_q\| \|x_s\|}, q, s \in \{1, 2, \dots, HW\} \quad (1)$$

where H and W are the height and width, respectively, of the query feature maps. Then, C_Q is normalized to between 0 and 1 as

$$C_Q = \frac{C_Q - \min(C_Q)}{\max(C_Q) - \min(C_Q) + \varepsilon} \quad (2)$$

where ε is a constant, which is set to $1e-7$. After all the inputs are obtained, they are concatenated along the channel dimension. Thus, the channel dimension becomes $256+256+1$. Then, we compress it to 256 dimensions with a 1×1 convolution operation. As indicated in Fig. 3, this branch consists of three convolutional blocks. The integrated feature maps are first interpolated to size $S \times S$; then, the probability that each grid cell represents the foreground or background is output through the convolutional blocks.

In the few-shot setting, we conduct the same process with PFENet [Tian et al., 2020]. The support prototypes and correlation maps that are produced by different support features are simply replaced by their mean values. Using this

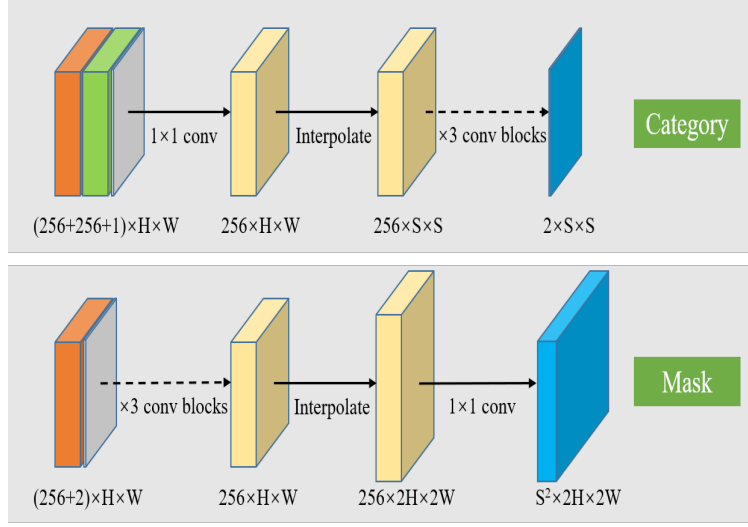


Figure 3: Architectures of the category branch and the mask branch. Each branch is mainly composed of three convolutional blocks. The category branch converts three inputs (the query feature maps, the expanded prototype and the normalized correlation map) into categories that correspond to each grid cell. The mask branch obtains the masks of the objects in each grid cell by combining the query features and the spatial coordinate information.

simple process, we achieve an obvious accuracy improvement compared to 1-shot segmentation without increasing the number of parameters of the model (see Table 1).

4.2 Mask branch

As discussed above, we divide each query image into an $S \times S$ grid. The purpose of the mask branch is to predict a binary mask for each grid cell. We stack all the masks together along the channel dimension; hence, the channel dimension of the output will be S^2 . The k^{th} channel represents the mask of the object in grid cell (i, j) , where $k = i * S + j, i, j \in \{0, 1, \dots, S - 1\}$. As shown in Fig. 3, we also use an FCN with three convolutional blocks to achieve this goal. However, the traditional convolution operation is spatially invariant, which is not desirable for our model because we need the model to be sensitive to the spatial information to obtain the masks of the objects that are located in each grid. Therefore, inspired by the CoordConv solution [Liu et al., 2018], we directly splice the x and y coordinate information and the query feature maps together to enable the convolutional filters to know their spatial locations. Thus, the third dimension of the new tensor becomes $D+2$, where D is the channel dimension of the query feature maps. Moreover, to prevent coordinate values that are too large from affecting the training of the model, they are normalized to $[-1, 1]$. Then, we use the convolutional blocks to extract object features. The output is upsampled to twice the size of the original feature maps to obtain more accurate masks. Finally, a 1×1 convolution operation is employed to generate S^2 masks.

4.3 Loss function

The loss function that we use consists of two parts: a pixel loss and a grid loss. The pixel loss is a cross-entropy loss that is calculated between the final prediction and the ground truth. It is defined as

$$L_{pixel} = -\frac{1}{N} \sum_{i=1}^N y_i \log p_i \quad (3)$$

where p_i and y_i denote the prediction and label, respectively, of pixel i and N is the total number of pixels.

However, we observe that only calculating the pixel loss cannot result in satisfactory performance (see Table 1). This is because in this approach, there are no additional constraints on the two branches, and it is essentially the same as the common pixel-wise classification methods. Therefore, to ensure that the two branches can play their respective roles, we calculate a grid loss for the category branch. We assume that the more pixels there are of the target object in a grid cell, the greater the probability that the mask that corresponds to this grid cell belongs to the foreground. For each

query mask, we first calculate the mean value of each grid G_m and then normalize it to [0,1] as follows:

$$G_m = \frac{G_m - \min(G_m)}{\max(G_m) - \min(G_m) + \varepsilon} \quad (4)$$

where ε is set to the same value as Eq. (2). The grid loss L_{grid} is defined as

$$L_{grid} = -\frac{1}{S^2} \sum_{i=1}^{S^2} G_{m,i} \log(\text{soft max}(g_i)) \quad (5)$$

where g_i represents the category of the i^{th} grid cell that is predicted by the category branch. Thus, the final loss function is expressed as

$$L = L_{pixel} + \lambda L_{grid} \quad (6)$$

where λ is a constant and is set to 1 in our experiments.

5 Experiments

5.1 Datasets and evaluation metrics

Two FSS benchmarks, namely, PASCAL-5ⁱ and COCO-20ⁱ, are selected to evaluate our method. PASCAL-5ⁱ is composed of PASCAL VOC 2012 Everingham et al. [2010] and extra annotations from the SDS Hariharan et al. [2014] dataset. It contains a total of 20 object categories and is evenly divided into four folds. For each fold, 15 classes are used for training, and the remaining 5 classes are used for testing. The COCO-20ⁱ dataset, which is built from MS-COCO [Lin et al., 2014], is a more challenging dataset that consists of 80 object categories. Likewise, all the classes are split into 4 folds. Thus, each fold has 20 classes. For each fold, 60 base classes are used for training, and the remaining 20 classes are used for testing.

Following the work of Shaban et al. [2017], the mean intersection over union (mIoU) is adopted as our main evaluation metric. It is calculated by averaging the IoUs of all the categories. Moreover, FB-IoU is also computed, which can measure the model’s ability to distinguish the foreground and the background. For PASCAL-5ⁱ, we randomly sample 1,000 episodes and calculate the average of the five runs as the final mIoU/FB-IoU. For COCO-20ⁱ, because of its large size, 20,000 episodes are sampled randomly to obtain stable results.

5.2 Implementation details

Our model is implemented with PyTorch on a single RTX 3080. We employ ResNet-50 and ResNet-101 as the backbones, which are pre-trained on ImageNet [Krizhevsky et al., 2012]. The parameters of the pre-trained backbone networks are frozen when the model is under training. Adam is leveraged to optimize the model, and the learning rate is set to 1e-4. All the images are resized to 473×473 pixels before they are fed to the model. During inference, the size of the output mask is recovered to the original size of the corresponding query images. Several data augmentation strategies, such as horizontal flipping, random scaling, random rotation and random shifting, are utilized. We set the batch size to 4 and train our model for 100 and 20 epochs on PASCAL-5ⁱ and COCO-20ⁱ, respectively. Notably, we directly output the final prediction result without fine-tuning or any other post-processing methods (e.g., DenseCRF [Chen et al., 2017]).

5.3 Results and analysis

Table 1 presents the mIoU and FB-IoU values that are obtained by our model on PASCAL-5ⁱ. We build our model on two backbones, namely, ResNet-50 and ResNet-101, and compare it with various state-of-the-art methods. When the model is built on ResNet-101, the mIoU values of the 1-shot and 5-shot experiments are 0.4% and 3.7% higher, respectively, than those on PFENet [Tian et al., 2020]. Notably, our model does not use multi-scale features and has only 5.5 M trainable parameters, but it can outperform the compared methods. In terms of FB-IoU, our model outperforms PFENet regardless of whether it uses ResNet -50 or ResNet -101 as the backbone in the 5-shot experiments. We also report the performance without using the grid loss. When the grid loss is not used in the training process, the performances in the 1-shot and 5-shot experiments severely deteriorate. In addition, the results of 5-shot segmentation are no longer significantly improved compared to those of 1-shot segmentation. This is probably because the model is not guided to extract the correct mask and it degenerates into a per-pixel classification model.

The experimental results on COCO-20ⁱ are presented in Table 2. It is obvious that our MANet achieves a higher mIoU than the state-of-the-art methods. It achieves 4.0% (1-shot) and 6.8% (5-shot) mIoU improvements over PFENet [Tian et al., 2020] using the ResNet-50 backbone. Due to the wide variety and the large differences in object scales of

Table 1: mIoU and FB-IoU of 1-shot and 5-shot segmentation on the PASCAL-5ⁱ dataset using the proposed method and state-of-the-art few-shot segmentation methods. Params represents the number of learnable parameters. † indicates that the grid loss is not used during training. The best performances and the minimum parameters are highlighted in bold.

Backbone	Method	1-shot						5-shot						Params
		Fold0	Fold1	Fold2	Fold3	Mean	FB-IoU	Fold0	Fold1	Fold2	Fold3	Mean	FB-IoU	
ResNet-50	PANet Wang et al. [2019]	44.0	57.5	50.8	44.4	49.1	66.5	55.3	67.2	61.3	53.2	59.3	70.7	14.7 M
	CANet [Zhang et al., 2019]	52.5	65.9	51.3	51.9	55.4	66.2	55.5	67.8	51.9	53.2	57.1	69.6	19.0 M
	PFENet [Tian et al., 2020]	61.7	69.5	55.4	56.3	60.8	72.0	63.1	70.7	55.8	57.9	61.9	72.3	10.4 M
	RePRI [Boudiaf et al., 2021]	60.2	67.0	61.7	47.5	59.1	-	64.5	70.8	71.7	60.3	66.8	-	-
	SCL [Zhang et al., 2021]	63.0	70.0	56.5	57.7	61.8	71.9	64.5	70.9	57.3	58.7	62.9	72.8	-
	MANet(Ours)	62.0	69.4	51.8	58.2	60.3	71.4	66.0	71.6	55.1	64.5	64.3	75.2	5.5 M
ResNet-101	PPNet [Liu et al., 2020b]	52.7	62.8	57.4	47.7	55.2	70.9	60.3	70.0	69.4	40.7	65.1	77.5	50.5 M
	FWB [Nguyen and Todorovic, 2019]	51.3	64.5	56.7	52.2	56.2	-	54.8	67.4	62.2	55.3	59.9	-	43.0 M
	DAN [Wang et al., 2020b]	54.7	68.6	57.8	51.6	58.2	71.9	57.9	69.0	60.1	54.9	60.5	72.3	-
	PFENet [Tian et al., 2020]	61.7	69.5	55.4	56.3	60.8	72.9	63.1	70.7	55.8	57.9	61.9	73.5	10.8 M
	RePRI [Boudiaf et al., 2021]	56.9	68.6	62.2	47.2	59.4	-	66.2	71.4	67.0	57.7	65.6	-	-
	MANet†(Ours)	64.0	68.1	52.2	57.0	60.3	70.9	64.1	69.2	52.3	56.5	60.5	71.0	5.5 M
	MANet(Ours)	63.9	69.2	52.5	59.1	61.2	71.4	67.0	70.8	54.8	65.5	64.5	74.1	5.5 M

Table 2: mIoU of 1-shot and 5-shot segmentation on the COCO-20ⁱ dataset using the proposed method and state-of-the-art few-shot segmentation methods. The best performances are highlighted in bold.

Backbone	Method	1-shot					5-shot				
		Fold1	Fold2	Fold3	Fold4	Mean	Fold1	Fold2	Fold3	Fold4	Mean
ResNet-50	FWB Nguyen and Todorovic [2019]	19.9	18.0	21.0	28.9	21.2	19.1	21.5	23.9	30.7	23.7
	PRMM [Yang et al., 2020b]	29.5	36.8	28.9	27.0	30.6	33.8	42.0	33.0	33.3	35.5
	PPNet [Liu et al., 2020b]	28.1	30.8	29.5	27.7	29.0	39.0	40.8	37.1	37.3	38.5
	PFENet [Tian et al., 2020]	34.3	33.0	32.3	30.1	32.4	38.5	38.6	38.2	34.3	37.4
	RePRI [Boudiaf et al., 2021]	31.2	38.1	33.3	33.0	34.0	38.5	46.2	40.0	43.6	42.1
	MANet(Ours)	33.9	40.6	35.7	35.2	36.4	41.9	49.1	43.2	42.7	44.2

this dataset, 1-shot segmentation fails when the support features are ambiguous. However, when 5-shot segmentation is performed, the model obtains the category of each mask more accurately by averaging all the support features. Therefore, in the 5-shot experiment, a 7.8% mIoU improvement over the 1-shot experiment is realized.

Fig. 4 shows several qualitative results of our model. The evaluation samples are from PASCAL-5ⁱ. We visualize and compare the results of MANet with the case in which the grid loss is not used. We observe that the masks that are generated by the model with the grid loss are more complete. Moreover, it is obvious that the grid loss enables the model to classify the masks more accurately. In contrast, MANet fails to obtain accurate object boundaries when the grid loss is not utilized. This is probably because when there is no restriction on the content that is generated by each grid cell, excessive training causes network overfitting. Thus, it gradually becomes a per-pixel classifier, which is vulnerable to boundary noise.

5.4 Ablation study of grid size

The proposed MANet aims to generate a fixed number of masks and integrate them according to their spatial locations. Therefore, the grid size is an important parameter of the model. In this section, we study the influence of it on the model. We conduct an ablation study on PASCAL-5ⁱ using ResNet-50 as the backbone. We divide the query images into grids of various sizes (12×12, 24×24, and 36×36). Both 1-shot and 5-shot experiments are conducted for comparison. Table 3 presents the mIoU and FB-IoU values for various grid sizes in the proposed MANet. We observe that the performance of the model is not greatly affected by the grid size. The result that is obtained using a 12×12 grid is equivalent to that obtained using a 36×36 grid but requires fewer calculations. This is probably because there are fewer small objects in the PASCAL-5ⁱ dataset and a 12×12 grid is sufficient for extracting most objects.

Table 3: Ablation study of grid size on PASCAL-5ⁱ

Grid Number	1-shot		5-shot	
	mIoU	FB-IoU	mIoU	FB-IoU
12×12	60.3	71.4	64.3	75.2
24×24	59.9	71.4	64.6	75.2
36×36	59.3	71.1	64.7	75.0

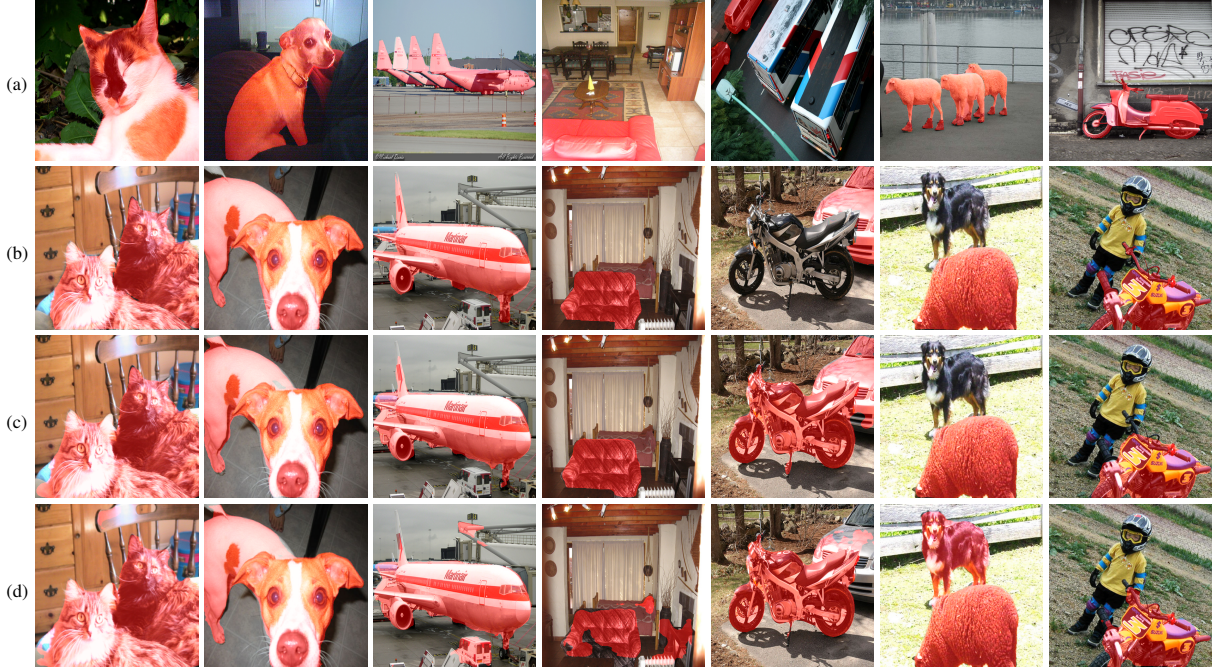


Figure 4: Qualitative results on our MANet on PASCAL-5ⁱ dataset. From top to bottom: (a) Support images for the 1-shot task and their masks; (b) the query images and their masks, (c) the predictions of MANet, and (d) the predictions of MANet without the grid loss.

5.5 Visualization of masks

To better understand why our method is effective, we visualize the concrete masks that are generated by the model with a grid of size 12×12 . In Fig. 5, we show all 144 masks of a query image that are produced by the mask branch at the corresponding positions. Subfigure (i,j) is the binary mask of the k^{th} channel dimension of the mask tensor, where $k = i * S + j, i, j \in \{0, 1, \dots, S - 1\}$. To clearly present the contents of the masks, we only show the masks that are predicted to correspond to the foreground by the category branch because the masks that are judged as corresponding to the background will not contribute to the segmentation result. We observe that each grid cell generates a mask for the objects that are located in it, and the mask that is produced by each grid cell is highly correlated with its location. Therefore, the final prediction result can be easily obtained by aggregating all the foreground masks.

6 Conclusions

We have presented a novel framework for few-shot semantic segmentation that is based on mask classification in this paper. The proposed MANet transforms FSS into a problem of classifying objects in each region by generating a set of binary masks. The segmentation result is obtained by assigning a category to each mask and aggregating all the masks that are predicted to correspond to the foreground. Leveraging a well-designed loss function, MANet can accurately extract the target masks through a simple two-branch structure. Experiments on the PASCAL-5ⁱ and COCO-20ⁱ datasets demonstrate that MANet outperforms the state-of-the-art pixel-based FSS methods. In addition to obtaining highly satisfactory results, it has very few parameters and is easy to combine with other methods. Therefore, we believe that the mask classification approach can be a potential baseline method for few-shot semantic segmentation.

References

- Y. Lecun and L. Bottou. Gradient-based learning applied to document recognition. *Proceedings of the IEEE*, 86(11): 2278–2324, 1998.
- J. Long, E. Shelhamer, and T. Darrell. Fully convolutional networks for semantic segmentation. *IEEE Transactions on Pattern Analysis and Machine Intelligence*, 39(4):640–651, 2015.

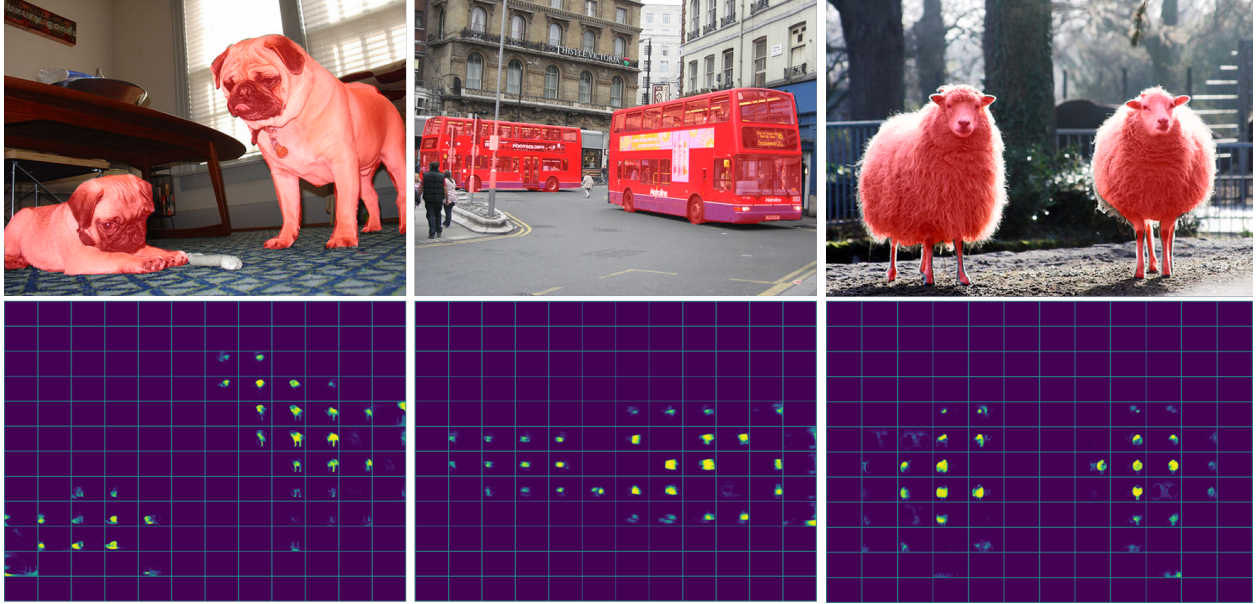


Figure 5: Visualization of generated masks. The top row presents query images and corresponding segmentation results. The bottom row shows all the masks that are produced by the mask branch of the model. The grid size is 12×12 ; thus, the total number of masks is 144. Each subfigure represents the mask that is generated at the corresponding location. To facilitate observation, we only show the foreground masks that affect the segmentation results.

Olaf Ronneberger, Philipp Fischer, and Thomas Brox. U-net: Convolutional networks for biomedical image segmentation. In *International Conference on Medical image computing and computer-assisted intervention*, pages 234–241. Springer, 2015.

Vijay Badrinarayanan, Alex Kendall, and Roberto Cipolla. Segnet: A deep convolutional encoder-decoder architecture for image segmentation. *IEEE transactions on pattern analysis and machine intelligence*, 39(12):2481–2495, 2017.

Hengshuang Zhao, Jianping Shi, Xiaojuan Qi, Xiaogang Wang, and Jiaya Jia. Pyramid scene parsing network. In *Proceedings of the IEEE conference on computer vision and pattern recognition*, pages 2881–2890, 2017.

Jun Fu, Jing Liu, Haijie Tian, Yong Li, Yongjun Bao, Zhiwei Fang, and Hanqing Lu. Dual attention network for scene segmentation. In *Proceedings of the IEEE/CVF Conference on Computer Vision and Pattern Recognition*, pages 3146–3154, 2019.

Amirreza Shaban, Shray Bansal, Zhen Liu, Irfan Essa, and Byron Boots. One-shot learning for semantic segmentation. In *proceedings of the British Machine Vision Conference*, pages 6230–6239, 2017.

Chi Zhang, Guosheng Lin, Fayao Liu, Rui Yao, and Chunhua Shen. Canet: Class-agnostic segmentation networks with iterative refinement and attentive few-shot learning. In *Proceedings of the IEEE/CVF Conference on Computer Vision and Pattern Recognition*, pages 5217–5226, 2019.

Kaixin Wang, Jun Hao Liew, Yingtian Zou, Daquan Zhou, and Jiashi Feng. Panet: Few-shot image semantic segmentation with prototype alignment. In *Proceedings of the IEEE/CVF International Conference on Computer Vision*, pages 9197–9206, 2019.

Zhuotao Tian, Hengshuang Zhao, Michelle Shu, Zhicheng Yang, Ruiyu Li, and Jiaya Jia. Prior guided feature enrichment network for few-shot segmentation. *IEEE Transactions on Pattern Analysis & Machine Intelligence*, 2020.

Yuwei Yang, Fanman Meng, Hongliang Li, Qingbo Wu, Xiaolong Xu, and Shuai Chen. A new local transformation module for few-shot segmentation. In *International Conference on Multimedia Modeling*, pages 76–87. Springer, 2020a.

Weide Liu, Chi Zhang, Guosheng Lin, and Fayao Liu. Crnet: Cross-reference networks for few-shot segmentation. In *Proceedings of the IEEE/CVF Conference on Computer Vision and Pattern Recognition*, pages 4165–4173, 2020a.

- Bolei Zhou, Aditya Khosla, Agata Lapedriza, Aude Oliva, and Antonio Torralba. Learning deep features for discriminative localization. In *Proceedings of the IEEE conference on computer vision and pattern recognition*, pages 2921–2929, 2016.
- Kaiming He, Georgia Gkioxari, Piotr Dollár, and Ross Girshick. Mask r-cnn. In *Proceedings of the IEEE international conference on computer vision*, pages 2961–2969, 2017.
- Bharath Hariharan, Pablo Arbeláez, Ross Girshick, and Jitendra Malik. Simultaneous detection and segmentation. In *European conference on computer vision*, pages 297–312. Springer, 2014.
- Alexander Kirillov, Kaiming He, Ross Girshick, Carsten Rother, and Piotr Dollár. Panoptic segmentation. In *Proceedings of the IEEE/CVF Conference on Computer Vision and Pattern Recognition*, pages 9404–9413, 2019.
- Bowen Cheng, Alex Schwing, and Alexander Kirillov. Per-pixel classification is not all you need for semantic segmentation. *Advances in Neural Information Processing Systems*, 34, 2021.
- Liang-Chieh Chen, Yukun Zhu, George Papandreou, Florian Schroff, and Hartwig Adam. Encoder-decoder with atrous separable convolution for semantic image segmentation. In *Proceedings of the European conference on computer vision (ECCV)*, pages 801–818, 2018.
- Hyeonwoo Noh, Seunghoon Hong, and Bohyung Han. Learning deconvolution network for semantic segmentation. In *Proceedings of the IEEE international conference on computer vision*, pages 1520–1528, 2015.
- Nanqing Dong and Eric P Xing. Few-shot semantic segmentation with prototype learning. In *proceedings of the British Machine Vision Conference*, volume 3, 2018.
- Xinlong Wang, Tao Kong, Chunhua Shen, Yuning Jiang, and Lei Li. Solo: Segmenting objects by locations. In *European Conference on Computer Vision*, pages 649–665. Springer, 2020a.
- Nicolas Carion, Francisco Massa, Gabriel Synnaeve, Nicolas Usunier, Alexander Kirillov, and Sergey Zagoruyko. End-to-end object detection with transformers. In *European Conference on Computer Vision*, pages 213–229. Springer, 2020.
- Kaiming He, Xiangyu Zhang, Shaoqing Ren, and Jian Sun. Deep residual learning for image recognition. In *Proceedings of the IEEE conference on computer vision and pattern recognition*, pages 770–778, 2016.
- Alex Krizhevsky, Ilya Sutskever, and Geoffrey E Hinton. Imagenet classification with deep convolutional neural networks. *Advances in neural information processing systems*, 25:1097–1105, 2012.
- Joseph Redmon, Santosh Divvala, Ross Girshick, and Ali Farhadi. You only look once: Unified, real-time object detection. In *Proceedings of the IEEE conference on computer vision and pattern recognition*, pages 779–788, 2016.
- Rosanne Liu, Joel Lehman, Piero Molino, Felipe Petroski Such, Eric Frank, Alex Sergeev, and Jason Yosinski. An intriguing failing of convolutional neural networks and the coordconv solution. *Advances in Neural Information Processing Systems*, 31, 2018.
- Mark Everingham, Luc Van Gool, Christopher KI Williams, John Winn, and Andrew Zisserman. The pascal visual object classes (voc) challenge. *International journal of computer vision*, 88(2):303–338, 2010.
- Tsung-Yi Lin, Michael Maire, Serge Belongie, James Hays, Pietro Perona, Deva Ramanan, Piotr Dollár, and C Lawrence Zitnick. Microsoft coco: Common objects in context. In *European conference on computer vision*, pages 740–755. Springer, 2014.
- Liang-Chieh Chen, George Papandreou, Iasonas Kokkinos, Kevin Murphy, and Alan L Yuille. Deeplab: Semantic image segmentation with deep convolutional nets, atrous convolution, and fully connected crfs. *IEEE transactions on pattern analysis and machine intelligence*, 40(4):834–848, 2017.
- Malik Boudiaf, Hoel Kervadec, Ziko Imtiaz Masud, Pablo Piantanida, Ismail Ben Ayed, and Jose Dolz. Few-shot segmentation without meta-learning: A good transductive inference is all you need? In *Proceedings of the IEEE/CVF Conference on Computer Vision and Pattern Recognition*, pages 13979–13988, 2021.
- Bingfeng Zhang, Jimin Xiao, and Terry Qin. Self-guided and cross-guided learning for few-shot segmentation. In *Proceedings of the IEEE/CVF Conference on Computer Vision and Pattern Recognition*, pages 8312–8321, 2021.
- Yongfei Liu, Xiangyi Zhang, Songyang Zhang, and Xuming He. Part-aware prototype network for few-shot semantic segmentation. In *European Conference on Computer Vision*, pages 142–158. Springer, 2020b.
- Khoi Nguyen and Sinisa Todorovic. Feature weighting and boosting for few-shot segmentation. In *Proceedings of the IEEE/CVF International Conference on Computer Vision*, pages 622–631, 2019.
- Haochen Wang, Xudong Zhang, Yutao Hu, Yandan Yang, Xianbin Cao, and Xiantong Zhen. Few-shot semantic segmentation with democratic attention networks. In *European Conference on Computer Vision*, pages 730–746. Springer, 2020b.

Boyu Yang, Chang Liu, Bohao Li, Jianbin Jiao, and Qixiang Ye. Prototype mixture models for few-shot semantic segmentation. In *European Conference on Computer Vision*, pages 763–778. Springer, 2020b.